

DNA entropic elasticity for short molecules attached to beads

Jinyu Li

Department of Applied Mathematics,
University of Colorado at Boulder, Boulder, CO

Philip C. Nelson

Department of Physics and Astronomy
University of Pennsylvania, Philadelphia, PA

M. D. Betterton¹

Department of Physics,
University of Colorado at Boulder, Boulder, CO

¹Corresponding author. Address: Department of Physics, University of Colorado at Boulder 390 UCB, Boulder, CO 80309 U.S.A., Tel.: (303)735-6235, Fax: (303)492-4066

Abstract

Single-molecule experiments in which force is applied to DNA or RNA molecules have enabled important discoveries of nucleic acid properties and nucleic acid-enzyme interactions. These experiments rely on a model of the polymer force-extension behavior to calibrate the experiments; typically the experiments use the worm-like chain (WLC) theory for double-stranded DNA and RNA. This theory agrees well with experiments for long molecules. Recent single-molecule experiments have used shorter molecules, with contour lengths in the range of 1-10 persistence lengths. Most WLC theory calculations to date have assumed infinite molecule lengths, and do not agree well with experiments on shorter chains. Key physical effects that become important when shorter molecules are used include *(i)* boundary conditions which constrain the allowed fluctuations at the ends of the molecule and *(ii)* rotational fluctuations of the bead to which the polymer is attached, which change the apparent extension of the molecule. We describe the finite worm-like chain (FWLC) theory, which takes into account these effects. We show the FWLC predictions diverge from the classic WLC solution for molecules with contour lengths a few times the persistence length. Thus the FWLC will allow more accurate experimental calibration for relatively short molecules, facilitating future discoveries in single-molecule force microscopy.

Key words: worm-like chain; single-molecule experiments; DNA; RNA; force-extension measurements; short chains; molecular stretching experiments; persistence length; contour length

Introduction

Single-molecule force microscopy, in which force is applied to DNA or RNA molecules one at a time, has enabled important discoveries of the mechanical behavior of nucleic acid (NA) molecules and NA-enzyme interactions (1, 2). These experiments are usually calibrated and interpreted using the worm-like chain theory (WLC). The WLC predicts the average end-to-end extension z of a semiflexible polymer, given the force F applied to the ends of the chain and the values of two constant parameters. The first parameter is the molecule's unstressed total contour length L , which is proportional to the number of base pairs in a double-stranded nucleic acid polymer. The second parameter, the effective bending stiffness parameter or persistence length A , describes the molecule's local elastic behavior. Hence we expect the value of A to depend on the molecule type and the nature of the surrounding solution, but not on the contour length. (Additional parameters enter when the stretching force exceeds about 20 pN, or when the molecule is torsionally constrained.) The WLC has been successfully applied to long molecules of DNA (3, 4) and RNA (5, 6) and it is now the standard model used in calibrating and interpreting SM force microscopy (7).

Existing treatments of the WLC theory do not agree well with experiments when the contour lengths of the NA molecules are short. In particular, experiments on dsDNA molecules with $L/A \sim 1$ –10 yield fit values of the persistence length which are physically unrealistic (8, 9, 10). These apparent values differ from the accepted value, $A \approx 50$ nm, by factors of 2–5. However, the persistence length is a material parameter, independent of the contour length. Therefore this apparent L -dependent persistence length amounts to a failure of the WLC, or at least its usual mathematical treatment, which assumes that $L \gg A$. In addition, the classic WLC solution neglects some physical effects present in the experiments, including the bead(s) attached to the end(s) of the molecule and surface effects. In this paper we extend the WLC to include boundary conditions at the ends of the polymer and rotational fluctuations of the bead(s) attached to the molecule, and present solutions valid at finite L . Our “finite worm-like chain” (FWLC) solution gives more accurate predictions than the classic WLC solution for polymers with contour lengths less than a few times the persistence length. In related recent work, Kulic *et al.* have studied finite-length effects in the stretching of DNA with a kink(11); their results apply in the high-force limit. At the other extreme, references (12) and (13) give numerical results for the “tethered particle”, or zero-force, limit.

Need for extensions of the WLC

The interactions between proteins and nucleic acids are essential to cells. Processes such as transcription and translation, splicing, DNA copying, genome maintenance and DNA repair require NA-protein interactions. Premature aging, cancer, and even death can result from defects in NA-protein interactions. (We use the abbreviation NA to refer to single- or

double-stranded DNA, RNA or DNA-RNA hybrid molecules). Single-molecule experiments have given new insight into NA-protein interactions, yielding information that is difficult to determine by other methods (1). In single-molecule force microscopy, force is applied to assess NA mechanical behavior or NA-protein interactions (14). Typically one end of an NA molecule is chemically attached to a surface and the other end is attached to a bead (figure 1). Manipulation of the bead, usually by optical (15) or magnetic (16) means, stretches the NA polymer. (In variants of this setup, the NA may be attached to beads at both ends, or an NA-binding protein may be attached to a surface.) Changes in the NA molecule extension and force can be measured or applied.

A theory of NA stretching behavior is required to calibrate single-molecule force experiments. The average end-to-end extension z of a polymer depends on the applied force F . Using an accurate model of the force-extension behavior means that once the calibration is performed, knowledge of any two of the extension, force, and contour length determines the other. Thus, changes in experimentally measured extension at fixed force can be directly related to changes in contour length, for example when a processive enzyme “reels in” NA as it moves.

In the absence of an accurate model of NA force-extension behavior, single-molecule force microscopy encounters several problems. First, experimentalists lack a check on whether the trap calibration is correct. Second, without an accurate force-extension theory, the contour length cannot be deduced from a measurement of the extension at fixed force. Therefore motion of motors which change the length of the polymer in time cannot be accurately measured. Third, force-extension measurements are frequently used to assess the number of polymers attached to a given bead. The attachment of polymers to the surface/bead occurs stochastically and can give more tethering molecules than desired. Measurement of the force-extension behavior is used to confirm the correct number of tether molecules. Fourth, experiments which study forced unfolding of secondary structure (8, 9, 17) require force-extension calibration to determine the free energy of the folded molecule.

The worm-like chain theory (WLC) of NA elasticity has become the standard model for calibrating experiments. The WLC assumes that the polymer is an infinitely long, inextensible, isotropic rod with bending rigidity. The usual WLC solution gives the relationship between fractional extension z/L and force in the limit $L \rightarrow \infty$ (2, 3, 7). However, physical effects neglected in the usual treatment of the WLC are important for relatively short molecules, such as those used in several experiments (8, 9, 10, 17, 18).

Experiments have fit data to the usual solution to the WLC even for relatively short chains, because no alternative treatment has been available (9, 10). The result is a fit value of the persistence length which depends on the contour length of the molecule, with fit values as low as 10 nm (9). For double-stranded DNA, the accepted value of the persistence length is approximately 50 nm (depending on solution conditions (19, 20)). Experimental force-extension data, when fit to a theory that correctly incorporates finite-length effects, should recover the intrinsic value of A , independent of L .

Finite-length effects can be incorporated into the WLC theory by considering boundary conditions at the end of the chain (11, 21). The constraints imposed by the boundary conditions alter the force-extension behavior. A second important physical effect typically neglected in the WLC theory is the rotational motion of the bead(s) attached to the molecule (figure 3). Experiments measure the position of the center of the bead, and typically one estimates the molecule extension by subtracting the bead radius. This estimate is correct only when the polymer-bead attachment is in line with the direction of the force ($\theta = 0$ in figure 3) and the bead undergoes no rotational fluctuations. For long molecules (with contour lengths of tens of μm), the fractional error introduced by subtracting the bead radius (typically 50–500 nm) can be neglected. However, for polymers with L of few hundred nanometers, the error caused by ignoring bead rotational fluctuations can be significant.

Several other physical effects are present in experiments, but neglected in most treatments of the WLC. These include (*i*) the exclusion interaction between the molecule and the surface (which prevents the polymer from entering the solid surface), (*ii*) the exclusion interaction between the bead and the surface, and (*iii*) the exclusion interaction between the molecule and the bead. These interactions are most important for zero or very low applied force, and have been addressed in recent work (12, 13, 22). Other interactions between the surface and the chain or bead may occur, such as electrostatic or van der Waals effects. In this paper, we will neglect these physical effects, which are important only for very low forces or very long polymers. Our goal in this paper is to present a unified model which includes the effects most important for single-molecule force microscopy experiments on dsDNA molecules with $L/A \sim 1\text{--}10$; for dsDNA this means contour lengths of 50–500 nm.

Theory

The WLC model assumes an inextensible polymer: the contour length L of the molecule (the total length of the molecular backbone) cannot be changed by applied force. For double-stranded DNA, the overstretching transition which occurs for applied force around 60 pN is a dramatic change in the organization of the molecule; however, lower applied forces (up to approximately 20 pN) respect the inextensibility constraint (23, 24). The polymer is assumed to possess an isotropic bending rigidity, characterized by the persistence length, A . The persistence length is the length scale over which thermal fluctuations randomize the chain orientation. (In principle, the rod also resists twist. However, in many experiments the twist is unconstrained and can be ignored.) We note that when considering single finite-length molecules, we are not working in any “thermodynamic limit”. Therefore, different ensembles are not guaranteed to be equivalent (25, 26, 27). In this paper we work in the ensemble relevant to most experiments, where the applied force is fixed and calculate the extension.

The chain energy includes the bending energy (Hooke’s law in the chain curvature) and

the work done by the applied force. The energy (in units of the thermal energy $k_B T$) is

$$E = -Fz + \int_0^L ds \frac{A}{2} \kappa^2 \quad (1)$$

Here F (the force divided by the thermal energy $k_B T$) is applied in the $\hat{\mathbf{z}}$ direction, s denotes arc length, and the total extension of the chain is z . The curvature can be defined in terms of arc-length derivatives of the chain coordinate (figure 2). If the chain conformation is described by a space curve $\mathbf{r}(s)$ and the unit vector tangent to the chain is $\hat{\mathbf{t}}(s)$, then $\kappa = \left| \frac{\partial^2 \mathbf{r}}{\partial s^2} \right| = \left| \frac{\partial \hat{\mathbf{t}}}{\partial s} \right|$. Note that the chain extension can be calculated as $z = \int_0^L ds \hat{\mathbf{z}} \cdot \hat{\mathbf{t}}$.

We rescale by dividing all lengths by the persistence length A , so the scaled energy is

$$E = \int_0^\ell ds' \left(\frac{\kappa'^2}{2} - f \hat{\mathbf{z}} \cdot \hat{\mathbf{t}} \right), \quad (2)$$

where $\ell = L/A$, $f = FA$, $s' = s/A$, and $\kappa' = \kappa A$. We will drop the primes in the remainder of the paper.

To determine the extension for a given applied force requires averaging over different polymer conformations. This leads to a path integral formulation of the statistical-mechanics problem in the tangent vector to the chain (28, 29). If the ends of the chain are held at fixed orientations, the partition function of the chain is

$$Z = \int D\hat{\mathbf{t}} \exp \left[- \int_0^\ell ds \left(\frac{1}{2} (\partial_s \hat{\mathbf{t}})^2 - f \hat{\mathbf{z}} \cdot \hat{\mathbf{t}} \right) \right], \quad (3)$$

where the integral in $D\hat{\mathbf{t}}$ is over all possible paths between the two endpoints of the chain with the specified orientations. The partition function can be rewritten as a propagator, which connects the probability distribution for the tangent vector at point s , $\psi(\hat{\mathbf{t}}, s)$ to the same probability distribution at point s' :

$$\psi(\hat{\mathbf{t}}, s) = \int d\hat{\mathbf{t}}' Z(\hat{\mathbf{t}}, s; \hat{\mathbf{t}}', s') \psi(\hat{\mathbf{t}}', s'). \quad (4)$$

From this relation, one can derive a Schrödinger-like equation which describes the s evolution of ψ (3):

$$\frac{\partial \psi}{\partial s} = \left(\frac{\nabla^2}{2} + f \cos \theta \right) \psi. \quad (5)$$

Here ∇^2 is the two-dimensional Laplacian on the surface of the unit sphere and $\cos \theta = \hat{\mathbf{z}} \cdot \hat{\mathbf{t}}$.

Additional physical effects included in the FWLC

Boundary conditions at ends of chain

For relatively short NA molecules, the boundary conditions at the ends of the chain must be considered (11, 21). The boundary conditions are specified by two probability density functions, $\psi(\hat{\mathbf{t}}, s = 0)$ and $\psi(\hat{\mathbf{t}}, s = L)$. These enter the full partition function via

$$Z_{tot} = \int d\hat{\mathbf{t}}_i d\hat{\mathbf{t}}_f \psi(\hat{\mathbf{t}}_i, 0) Z(\hat{\mathbf{t}}_i, 0; \hat{\mathbf{t}}_f, L) \psi(\hat{\mathbf{t}}_f, L). \quad (6)$$

Bead rotational fluctuations

Rotational fluctuations of the bead can be explicitly included in the theory. Here we describe the extension due to a bead at one end of the chain, with the other end of the chain held at fixed orientation (figure 1a; the generalization to consider beads at both ends of the polymer is straightforward). In this case, the theory predicts the extension to the center of the bead, not just the molecule extension. We assume that the bead is spherical and the fluctuations in the polymer-bead attachment are azimuthally symmetric about the $\hat{\mathbf{z}}$ axis (figure 3).

The unit vector $\hat{\mathbf{n}}$ points from the center of the bead to the polymer-bead attachment. Thus the bead's contribution to the energy of a fluctuation with a given $\hat{\mathbf{n}}$ is $FR\hat{\mathbf{n}} \cdot \hat{\mathbf{z}}$, where R is the bead radius. Note that the energy is minimized when $\hat{\mathbf{n}} = -\hat{\mathbf{z}}$, and for other bead orientations the energy increases. This gives a restoring torque on the bead which increases as FR increases. We write the rescaled energy including this term as

$$E = fr\hat{\mathbf{n}} \cdot \hat{\mathbf{z}} + \int_0^\ell ds \left(\frac{\kappa^2}{2} - f\hat{\mathbf{z}} \cdot \hat{\mathbf{t}} \right), \quad (7)$$

where $r = R/A$. The partition function of the chain is

$$Z = \int D\hat{\mathbf{t}} \exp \left[- \int_0^\ell ds \left(\frac{1}{2} (\partial_s \hat{\mathbf{t}})^2 - f\hat{\mathbf{z}} \cdot \hat{\mathbf{t}} \right) \right] \int_{\text{constr}} d\hat{\mathbf{n}} \exp(-fr\hat{\mathbf{n}} \cdot \hat{\mathbf{z}}), \quad (8)$$

where the first integral is over all possible paths between the two endpoints of the chain, and the second integral is over all allowable vectors $\hat{\mathbf{n}}$. Below we evaluate the second integral, thereby performing the average over fluctuations in $\hat{\mathbf{n}}$.

Methods

Here we describe the calculation of the force-extension relation, the main quantity of interest in single-molecule experiments. We must first calculate the tangent-vector probability distribution $\psi(\hat{\mathbf{t}}, s)$ for all s along the chain. The distribution satisfies equation (5) above. This

PDE can be solved using separation of variables in s and $\hat{\mathbf{t}}$, where the angular dependence is expanded in spherical harmonics (3).

$$\psi(\hat{\mathbf{t}}, s) = \sum_{j=0}^{\infty} \Psi_j(s) Y_{j0}(\hat{\mathbf{t}}). \quad (9)$$

We assume azimuthal symmetry, so only the $m = 0$ spherical harmonics, with no ϕ dependence, are included. In the basis of spherical harmonics, the operator in equation (5) is a symmetric tridiagonal matrix H with diagonal terms

$$H_{j,j} = -\frac{j(j+1)}{2}, \quad (10)$$

and off-diagonal terms

$$H_{j,j+1} = \frac{f(j+1)}{(2j+1)(2j+3)}. \quad (11)$$

The vector of coefficients at point s is given by the matrix exponential of H :

$$\mathbf{\Psi}(s) = e^{sH} \mathbf{\Psi}(0). \quad (12)$$

This expression allows us to compute the probability distribution of the tangent vector orientation at any point along the chain. This result is exact if the infinite series of spherical harmonics is used. In practice, the series must be truncated for numerical calculations. Our calculations use $N = 30$ unless otherwise specified.

The partition function is then calculated from the inner product

$$Z = \mathbf{\Psi}^T(s = \ell) e^{\ell H} \mathbf{\Psi}(s = 0), \quad (13)$$

$$= \sum_{j,k} \Psi_j(s = \ell) [e^{\ell H}]_{jk} \Psi_k(s = 0). \quad (14)$$

The extension at a given applied force is

$$\frac{z}{L} = \frac{1}{\ell} \frac{\partial \ln Z}{\partial f}. \quad (15)$$

This formula applies for a chain of any length.

Finite-length correction

To calculate the force-extension relation we must determine $M = e^{\ell H}$ [equations (12) and (14)]. Because H includes at least one positive eigenvalue, the entries M grows rapidly with ℓ . This increase can lead to numerical overflow errors when computing M . However, we are

interested not in the entries of the matrix but in the logarithmic derivative of the partition function, and a rescaling can avoid the overflow problem.

Let $A = e^H$ and denote by λ_* the largest eigenvalue of A . Then $M = A^\ell$. If we define $\mathcal{A} = A/\lambda_*$, we have $M = \lambda_*^\ell \mathcal{A}^\ell$. Thus \mathcal{A} has eigenvalues with magnitude less than or equal to 1. The partition function can be written

$$Z = \lambda_*^\ell \mathbf{\Psi}^T(s = \ell) \mathcal{A}^\ell \mathbf{\Psi}(s = 0). \quad (16)$$

The logarithm of the partition function is then

$$\ln Z = \ell \ln \lambda_* + \ln[\mathbf{\Psi}^T(s = \ell) \mathcal{A}^\ell \mathbf{\Psi}(s = 0)]. \quad (17)$$

In the usual WLC solution, only the first term is considered (3), an approximation which is exact in the limit $\ell \gg 1$. The second term is the correction to $\ln Z$ due to finite-length effects.

Boundary conditions

The boundary conditions at $s = 0$ and $s = \ell$ affect the force-extension relation, because they affect the partition function [equation (14)]. The functional form of a specific boundary condition is given by the vector of coefficients $\mathbf{\Psi}(s = 0)$, which is determined by the projection of $\psi(\hat{\mathbf{t}}, s)$ onto spherical harmonics. To apply different boundary conditions, we simply determine the partition function for different vectors $\mathbf{\Psi}(s = 0)$ and $\mathbf{\Psi}(s = \ell)$ (21).

In this paper, we consider three types of boundary conditions (figure 4). First, in the “unconstrained” boundary condition the tangent vector at the end of the chain is free to point in any direction on the sphere (in 4π of solid angle, figure 4a). In real experiments, however, the boundary conditions are more constrained. If the polymer is attached to a surface about a freely rotating attachment point, we might expect “half-constrained” boundary conditions (figure 4b), where the tangent vector at the end of the chain can point in any direction on the hemisphere outside the impenetrable surface. Many experiments appear to implement half-constrained boundary conditions, because they use a flexible attachment between the chain and the surface (13). We also consider perpendicular boundary conditions, where the tangent vector at the end of the chain is parallel to the $\hat{\mathbf{z}}$ axis, normal to the surface (figure 4c).

For the unconstrained boundary condition, $\psi(\hat{\mathbf{t}})$ is independent of $\cos \theta$. Therefore $\mathbf{\Psi} = (1, 0, \dots, 0)$. For the half-constrained boundary condition, the leading coefficients of $\mathbf{\Psi}$ are $(1, 0.8660, 0, -0.3307, 0, 0.2073, 0)$. Finally, for the perpendicular boundary condition the coefficients of $\mathbf{\Psi}$ are all equal to 1. (Note that for the computation of the force-extension relation, it is not necessary to properly normalize the probability distribution, because we are computing the derivative of the logarithm of Z . Our expressions for the probability distribution vectors will neglect the constant normalization factor.)

Bead rotational fluctuations

The bead rotational fluctuations lead to an effective boundary condition (at the end of the polymer) that depends on applied force and bead radius. For the single-bead experimental geometry (figure 1a), equation (8) gives the partition function of the system including bead rotational fluctuations. We can perform the integral over $\hat{\mathbf{n}}$ to find the probability distribution of $\hat{\mathbf{t}}(\ell)$, that is, is the effective boundary condition at the end of the polymer. The integral over $\hat{\mathbf{n}}$ is

$$g(\hat{\mathbf{t}}(\ell), \hat{\mathbf{z}}) = \int_{\text{constr}} d\hat{\mathbf{n}} e^{-fr\hat{\mathbf{n}}\cdot\hat{\mathbf{z}}}. \quad (18)$$

Because the direction of $\hat{\mathbf{n}}$ is constrained relative to the chain tangent $\hat{\mathbf{t}}(\ell)$, this integral is a function of $\hat{\mathbf{t}}(\ell)$. By azimuthal symmetry, it depends only on the scalar $\hat{\mathbf{t}}(\ell) \cdot \hat{\mathbf{z}}$. Accordingly we can express equation (18) in the form $g(\hat{\mathbf{t}}(\ell) \cdot \hat{\mathbf{z}})$, where g is the probability distribution of tangent angles at $s = \ell$. (Note that we neglect the normalization constant for g .) Expanding in spherical harmonics, we write

$$g(\hat{\mathbf{t}}(\ell) \cdot \hat{\mathbf{z}}) = g(\cos \gamma) = \sum_{j=0}^{\infty} \Psi_j(s = \ell) Y_{j0}(\gamma). \quad (19)$$

The effective boundary condition depends on both the applied force and the radius of the bead. The physical character of the chain-bead attachment determines the constraints in the integral of equation (18), and therefore controls the Ψ_j .

For the two-bead experimental geometry, the partition function includes integrals over bead rotational fluctuations for both ends of the chain, and the effective boundary condition applies at both ends of the polymer.

Half-constrained boundary conditions

Suppose that the polymer-bead attachment is half-constrained, so the tangent vector is free in a hemisphere (figure 4b). Then the integral of equation (18) is constrained by $\hat{\mathbf{t}}(\ell) \cdot \hat{\mathbf{n}} < 0$, or

$$g(\hat{\mathbf{t}} \cdot \hat{\mathbf{z}}) = \int_{\hat{\mathbf{t}}\cdot\hat{\mathbf{n}}<0} d\hat{\mathbf{n}} e^{-fr\hat{\mathbf{n}}\cdot\hat{\mathbf{z}}}. \quad (20)$$

To evaluate the integral, we choose a polar coordinate system where $\hat{\mathbf{t}} \cdot \hat{\mathbf{z}} = \cos \gamma$, $\hat{\mathbf{t}}$ points along the polar axis, and $\phi = 0$ corresponds to the $\hat{\mathbf{z}}$ direction. Therefore $\hat{\mathbf{z}} = (\sin \gamma, 0, \cos \gamma)$, $\hat{\mathbf{n}} = (\sin \theta \cos \phi, \sin \theta \sin \phi, \cos \theta)$, and $\hat{\mathbf{n}} \cdot \hat{\mathbf{z}} = \sin \theta \cos \phi \sin \gamma + \cos \theta \cos \gamma$. We can then write

g in terms of the Bessel function J_o .

$$g(\hat{\mathbf{t}} \cdot \hat{\mathbf{z}}) = \int_0^{2\pi} d\phi \int_{-1}^0 d\cos\theta e^{-fr(\sin\theta \cos\phi \sin\gamma + \cos\theta \cos\gamma)}, \quad (21)$$

$$= \int_{-1}^0 d\cos\theta e^{-fr \cos\theta \cos\gamma} \int_0^{2\pi} d\phi e^{-fr \sin\theta \cos\phi \sin\gamma}, \quad (22)$$

$$= 2\pi \int_{-1}^0 d\cos\theta e^{-fr \cos\theta \cos\gamma} J_o(-ifr \sin\theta \sin\gamma). \quad (23)$$

Note that $\int_0^\pi \exp(z \cos x) = \pi J_o(iz)$, and the integral from 0 to 2π is even about π . We show the values of this function in figure 5 for different applied forces and bead radii. As expected, for small applied force and small bead radius, the probability distribution approaches a constant value (independent of $\cos\gamma$). However, for large applied force, the probability distribution approaches the half-constrained distribution one would expect in the absence of bead rotational fluctuations.

Numerical methods

Because $\cos\theta$ is integrated over negative values in equation (23), the term $e^{-fr \cos\theta \cos\gamma}$ diverges as fr increases. However, we only calculate the dependence of g on $\cos\gamma$ (correct normalization is not required). Therefore we replace the term $e^{-fr \cos\theta \cos\gamma}$ in the integral with the term $e^{-fr(\cos\theta \cos\gamma + 1)}$.

To determine the effective boundary condition due to the rotationally fluctuating bead requires that we expand integrals of the form given in equation (23) in spherical harmonics. Direct numerical projection of the integral onto spherical harmonics leads to large errors, because numerical integration of rapidly oscillating functions (such as the higher-order spherical harmonics) is inaccurate. To solve this problem, we used an interpolating basis (reference (30), section 3.1.4). This allows the coefficients of the spherical harmonics to be determined by evaluation of equation (23) at specific points (corresponding to the zeros of the Legendre polynomials). The integral in equation (23) was evaluated numerically using Gauss-Legendre quadrature.

Results

Here we delineate the regimes where the usual WLC solution applies, and where the FWLC is required for good agreement with experiment. The classic WLC predictions becomes less accurate as the contour length of the chain decreases. The differences between the WLC and FWLC also depend on applied force, boundary conditions, and bead radius.

As expected, the FWLC predictions converge to the WLC predictions as the polymer contour length increases. Figure 6 shows the predicted fractional extension z/L as a function

of the chain contour length L (for fixed applied force). Predictions calculated from the classic WLC solution are independent of contour length. However, for the FWLC the predicted fractional extension deviates from the infinite value for smaller values of L . In all cases, the FWLC predictions converge to the classic WLC results as $L \rightarrow \infty$.

Error threshold contour length

To summarize the different predictions of the FWLC and WLC, we calculate the “error threshold contour length” L_e . As shown in figure 6, the FWLC and WLC predictions diverge as L is decreased. We decrease L and compare the FWLC and WLC predictions. The error threshold contour length L_e is defined as the contour length where the relative difference between the two predictions first reaches 5%. For contour lengths $L < L_e$ the FWLC model is necessary for accurate predictions. By characterizing the dependence of L_e on boundary conditions, applied force, and bead radius, we can understand which parameters control the difference between FWLC and WLC predictions.

Figure 7 shows the error threshold length as a function of applied force for different boundary conditions and bead radii. For all conditions described, L_e is largest for low applied force, where the predicted extension is most altered by finite-length effects. This behavior is intuitively reasonable. When the applied force tends to infinity, only one chain conformation is possible—the chain is perfectly straight, aligned in the direction of the force. In this case, modifying the theory to include boundary conditions or bead rotational fluctuations does not alter the polymer conformation. The characteristic propagation length of deformations in a classical elastic rod (that is, neglecting thermal fluctuations) is $\sqrt{A/F}$. As the force increases, the effects of any constraints on the ends of the polymer have decreasing effect on the conformation. Similarly, when the applied force is large bead rotational fluctuations require a large amount of energy and are suppressed.

When the applied force is low, many different chain conformations are probable. Therefore the boundary conditions and bead rotational fluctuations exert greater influence on the chain extension. Unconstrained boundary conditions maximize the number of allowable conformations. In this case the entropy is maximized, and the polymer extension is low: increasing the extension requires excluding many chain conformations, which requires more work. More constrained boundary conditions restrict the number of conformations that are possible, leading to lower entropy and therefore a larger extension. At low force, the most constrained boundary conditions typically lead to the largest extension. We illustrate this idea with the limit of a perfectly rigid rod which is constrained at one end to be perpendicular to the surface. The infinite rigidity means that the molecule must be perfectly straight. The boundary conditions require that the polymer take only one conformation, perpendicular to the surface. In other words, the boundary conditions severely restrict the number of available conformations, and thereby increase the predicted extension. (If the boundary conditions are unconstrained, the rod rotates to point in many different directions and its

average extension is lower). In addition, for low applied force bead rotational fluctuations are larger, leading to a larger alteration of the extension due to bead fluctuations.

Force-extension behavior

We illustrate the force-extension curves for different boundary conditions and contour lengths: $L/A = 4$ in figure 8 and $L/A = 10$ in figure 9. As described above, (i) the fractional difference between the infinite and finite predictions is largest for low contour lengths and low applied forces, (ii) the more constrained boundary conditions lead to the largest changes relative to the infinite model, and (iii) the more constrained boundary conditions typically lead to larger extensions at low force. Therefore, the force-extension curves for the FWLC with unconstrained boundary conditions are closest to the classic WLC predictions (figure 8).

Including bead rotational fluctuations in the model leads to an effective boundary condition that depends on applied force and bead radius, as shown in figure 5. The variation of the effective boundary condition with force alters the shape of the force-extension curve. For high applied force, the fluctuations require more energy and so large-angle fluctuations occur less frequently. Therefore, in the limit $FR \rightarrow \infty$ the probability distribution approaches that of the chain-bead attachment. However, for smaller FR , the bead rotational fluctuations “smear out” the probability distribution, making the effective tangent angle boundary condition approach a constant, independent of $\cos \gamma$. For smaller FR , the the predicted extension is similar to that expected for no bead and unconstrained boundary conditions. This typically leads to a smaller extension than would occur in the absence of a bead. For larger FR , the effective boundary condition approaches the boundary condition that would occur with no bead. In this case, there is little difference between the predicted extension with and without a bead.

We note that two opposing trends occur as the bead radius varies: when the bead is smaller, the fractional error made by subtracting R from the measured extension to estimate the molecule extension is smaller, simply because one is subtracting a smaller value. However, for smaller R the restoring torque on the bead for a given F is also smaller, which leads to larger angular fluctuations for smaller beads.

At very low forces our FWLC theory gives inaccurate predictions, because it does not explicitly include the exclusion interaction between the bead and the wall. If the force is very low, the predicted extension would imply that the bead overlaps with the wall (or the other bead). Typically we find that applied force > 0.08 pN is required to prevent predicted bead-wall overlap in our theory. Although the FWLC does lead to unphysical predictions at very low forces, the simple model of the bead rotational fluctuations is useful for larger values of the force.

Fitting FWLC curves to the classic WLC solution

Here we illustrate the typical errors that occur if one fits force-extension curves generated by the FWLC to the usual WLC solution. We generated force-extension data with the FWLC, and fit to the WLC solution of Bouchiat *et al* (7). We find that the contour length is typically fit well by the WLC model, but large errors in the fitted value of the persistence length occur. The apparent persistence length decreases with contour length (figure 10), as observed experimentally in the stretching of short DNA molecules (9). The magnitude of the error increases as the boundary conditions become more constrained, or when beads are included in the model.

We emphasize that our fitting result is not directly comparable to the fitting of experimental data, because our simulated “data” are not noisy. In fits of real data, the quality of the fit is affected by the amount of noise. However, our result does show the types of errors that occur: fitting “data” generated by the FWLC to the usual WLC solution leads to large errors in the persistence length for small L . By contrast, fitting to the FWLC recovers the correct value of A .

Discussion

In this paper we have developed the finite worm-like chain theory (FWLC), which predicts the force-elasticity behavior of polymers with short contour lengths ($\ell = L/A \sim 1-10$). In addition to retaining contributions from the subleading terms of equation (17), the FWLC includes two physical effects neglected in the usual WLC treatment: (*i*) chain-end boundary conditions and (*ii*) bead rotational fluctuations. Together, these effects may explain the apparent decrease in polymer persistence length which has been experimentally measured for short chains (9).

A key result of this paper is the delineation of the regimes where we expect the usual WLC solution to fail. We demonstrate that the FWLC converges to the WLC in the limit of long contour length for all forces, boundary conditions, and bead radii. However, for shorter molecules the contour length crossover where the usual WLC solution becomes inaccurate depends on applied force, chain-end boundary conditions, and bead radius. For the FWLC and WLC to agree within 5% for a force-extension measurement with applied force of 0.1–10 pN, requires $L/A > 100$ ($L > 5000$ nm for dsDNA).

Although the FWLC improves on the usual WLC solution for short contour lengths, it does not include all physical effects which occur in single-molecule force microscopy. In particular, effects omitted from the FWLC are important for very low or zero applied force (such as in tethered particle motion experiments). These effects include the chain-wall, chain-bead, and bead-wall exclusion interactions. All of these interactions are most important at zero applied force. In our calculations, the average position of the bead is “outside” the wall for forces above 0.1 pN. For accurate predictions at lower applied force, exclusion effects

need to be included. Comparison of the FWLC with models which include the exclusion interactions can further define the regimes of applicability of this model. In the future, an improved theory which also applies at very low force may become necessary.

The FWLC will be useful for experiments that use short NA polymers in single-molecule force microscopy. A theory that is correct for small L/A helps ensure that the experimental force calibration is correct, that least-squares fitting indeed recovers the correct values of the contour and persistence lengths, and that the number of polymers attached between surface and bead can accurately be determined. The FWLC will facilitate experimental work with shorter polymers and contribute to future discoveries in nucleic acid-enzyme interactions.

Acknowledgements

We thank Igor Kulic, Tom Perkins, Rob Phillips, and Michael Woodside for useful discussions, and the Aspen Center for Physics, where part of this work was done. PCN acknowledges support from NSF grant DMR-0404674 and the NSF-funded NSEC on Molecular Function at the Nano/Bio Interface, DMR-0425780. MDB acknowledges support from NSF NIRT grant PHY-0404286, the Butcher Foundation, and the Alfred P. Sloan Foundation.

References

1. Bustamante, C., J. C. Macosko, and G. J. L. Wuite. 2000. Grabbing the cat by the tail: Manipulating molecules one by one. *Nature Reviews Molecular Cell Biology* 1:130.
2. Nelson, P. 2004. *Biological Physics: Energy, Information, Life*. W. H. Freeman and Co., New York.
3. Marko, J. F., and E. D. Siggia. 1995. Stretching DNA. *Macromolecules* 28:8759.
4. Bustamante, C., J. F. Marko, E. D. Siggia, and S. Smith. 1994. Entropic elasticity of lambda-phage DNA. *Science* 265:1599.
5. Seol, Y., G. M. Skinner, and K. Visscher. 2004. Elastic properties of a single-stranded charged homopolymeric ribonucleotide. *Physical Review Letters* 93:118102.
6. Abels, J. A., F. Moreno-Herrero, T. van der Heijden, C. Dekker, and N. H. Dekker. 2005. Single-molecule measurements of the persistence length of double-stranded RNA. *Biophysical Journal* 88:2737.
7. Bouchiat, C., M. D. Wang, J. F. Allemand, T. Strick, S. M. Block, and V. Croquette. 1999. Estimating the persistence length of a worm-like chain molecule from force-extension measurements. *Biophysical Journal* 76:409.

8. Liphardt, J., B. Onoa, S. B. Smith, I. Tinoco, and C. Bustamante. 2001. Reversible unfolding of single RNA molecules by mechanical force. *Science* 292:733.
9. Onoa, B., S. Dumont, J. Liphardt, S. B. Smith, I. Tinoco, and C. Bustamante. 2003. Identifying kinetic barriers to mechanical unfolding of the T-thermophila ribozyme. *Science* 299:1892.
10. Perkins, T. T., H. W. Li, R. V. Dalal, J. Gelles, and S. M. Block. 2004. Forward and reverse motion of single RecBCD molecules on DNA. *Biophysical Journal* 86:1640.
11. Kubic, I. M., H. Mohrbach, V. Lobaskin, R. Thakar, and H. Schiessel. 2005. Apparent persistence length renormalization of bent DNA. *Physical Review E* 72:041905.
12. Segall, D. E., P. Nelson, and R. Phillips. 2005. Excluded-volume effects in tethered-particle experiments: Bead size matters. Submitted, <http://arxiv.org/abs/q-bio.BM/0508028>.
13. Nelson, P. C., D. Brogioli, C. Zurla, D. D. Dunlap, and L. Finzi. 2005. Quantitative analysis of tethered particle motion. Submitted.
14. Allemand, J. F., D. Bensimon, and V. Croquette. 2003. Stretching DNA and RNA to probe their interactions with proteins. *Current Opinion in Structural Biology* 13:266.
15. Neuman, K. C., and S. M. Block. 2004. Optical trapping. *Review of Scientific Instruments* 75:2787.
16. Gosse, C., and V. Croquette. 2002. Magnetic tweezers: Micromanipulation and force measurement at the molecular level. *Biophysical Journal* 82:3314.
17. Liphardt, J., S. Dumont, S. B. Smith, I. Tinoco, and C. Bustamante. 2002. Equilibrium information from nonequilibrium measurements in an experimental test of Jarzynski's equality. *Science* 296:1832.
18. Lang, M. J., P. M. Fordyce, A. M. Engh, K. C. Neuman, and S. M. Block. 2004. Simultaneous, coincident optical trapping and single-molecule fluorescence. *Nature Methods* 1:133.
19. Baumann, C. G., S. B. Smith, V. A. Bloomfield, and C. Bustamante. 1997. Ionic effects on the elasticity of single DNA molecules. *Proceedings of the National Academy of Sciences of the United States of America* 94:6185.
20. Wang, M. D., H. Yin, R. Landick, J. Gelles, and S. M. Block. 1997. Stretching DNA with optical tweezers. *Biophysical Journal* 72:1335.

21. Samuel, J., and S. Sinha. 2002. Elasticity of semiflexible polymers. *Physical Review E* 66:050801.
22. Bouchiat, C. 2005. A formulation of the worm like chain model appropriate to double-strand DNA subject to spatial constraints. <http://www.arxiv.org/abs/cond-mat/0501171>.
23. Smith, S. B., Y. J. Cui, and C. Bustamante. 1996. Overstretching B-DNA: The elastic response of individual double-stranded and single-stranded DNA molecules. *Science* 271:795.
24. Storm, C., and P. C. Nelson. 2003. The bend stiffness of S-DNA. *Europhysics Letters* 62:760.
25. Keller, D., D. Swigon, and C. Bustamante. 2003. Relating single-molecule measurements to thermodynamics. *Biophysical Journal* 84:733.
26. Sinha, S., and J. Samuel. 2005. Inequivalence of statistical ensembles in single molecule measurements. *Physical Review E* 71:021104.
27. Dhar, A., and D. Chaudhuri. 2002. Triple minima in the free energy of semiflexible polymers. *Physical Review Letters* 89:065502.
28. Fixman, M., and J. Kovac. 1973. Polymer conformational statistics. 3. Modified gaussian models of stiff chains. *Journal of Chemical Physics* 58:1564.
29. Yamakawa, H. 1976. Statistical-mechanics of wormlike chains. *Pure and Applied Chemistry* 46:135.
30. Alpert, B., G. Beylkin, D. Gines, and L. Vozovoi. 2002. Adaptive solution of partial differential equations in multiwavelet bases. *Journal of Computational Physics* 182:149.

Figure Legends

Figure 1.

Sketch of typical experimental geometries for single-molecule force microscopy with nucleic acid polymers. The total molecule extension is z . (a) One-bead geometry. The molecule is attached at one end to a surface (glass slide or coverslip) and at other end to a bead. Force is applied to the center of the bead. (b) Two-bead geometry. The molecule is attached at both ends to beads. Force is effectively applied to the centers of both beads.

Figure 2.

Variables used to describe chain conformations. Force is applied in the $\hat{\mathbf{z}}$ direction. The arc length along the chain is s , and the vector $\mathbf{r}(s) = (x(s), y(s), z(s))$ is the coordinate of the chain at arc length s . The vector $\hat{\mathbf{t}}(s)$ is the unit vector tangent to the chain at s .

Figure 3.

Variables used to describe bead rotational fluctuations. The vector $\hat{\mathbf{n}}$ points from the center of the bead to the polymer-bead attachment. The angle θ between the $\hat{\mathbf{z}}$ direction and the bead-chain attachment is defined by $\cos \theta = -\hat{\mathbf{n}} \cdot \hat{\mathbf{z}}$. The bead has radius R .

Figure 4.

Sketch of the tangent-angle boundary conditions. (a) Unconstrained boundary conditions. The tangent vector at the end of the chain (open arrowhead) can point in all directions relative to the $\hat{\mathbf{z}}$ axis (notched arrowhead) with equal probability. (b) Half-constrained boundary conditions. Due to a constraint (such as the presence of a solid surface normal to the $\hat{\mathbf{z}}$ axis) the tangent vector at the end of the chain can point only in the upper half-sphere. (c) Perpendicular boundary conditions. The tangent vector is constrained to point only normal to the surface, in the $\hat{\mathbf{z}}$ direction.

Figure 5.

Effective chain-end boundary conditions induced by bead rotational fluctuations. The unnormalized probability density $g(\hat{\mathbf{t}} \cdot \hat{\mathbf{z}})$ is shown versus $\cos \gamma = \hat{\mathbf{t}} \cdot \hat{\mathbf{z}}$. Top, bead radius $R = 100$ nm. Middle, bead radius $R = 250$ nm. Bottom, bead radius $R = 500$ nm. The different curves correspond to different values of the applied force. In this calculation the attachment of the chain to the bead is half-constrained: in the absence of bead rotational fluctuations, the probability density is zero for $\cos \gamma < 0$ and constant for $\cos \gamma > 0$. This step function is approached for large force and large R . For smaller values of FR the probability density is smeared out, and approaches a constant value (independent of $\cos \gamma$) for small FR .

Figure 6.

Convergence of the FWLC-predicted extension to the classic WLC prediction for large L . The predicted fractional extension z/L is shown as a function of the contour length L (at fixed applied force). The different curves correspond to different theoretical assumptions: (i) the classic WLC solution, calculated using the method of ref. (3), (ii) the FWLC with unconstrained boundary conditions, (iii) the FWLC with half-constrained boundary conditions, and (iv) the FWLC with perpendicular boundary conditions (see figure 4). The different panels show different applied forces: top, 0.01 pN; middle, 0.1 pN; bottom, 1 pN. The polymer persistence length is $A = 50$ nm. Note that the WLC prediction is independent of contour length, and the FWLC predictions converge to the WLC prediction as L increases. The convergence occurs more quickly for higher applied force (see text, note different y -axis scales for different panels). For low applied force, the more constrained boundary conditions lead to larger predicted fractional extension (see text).

Figure 7.

Error threshold length L_e as a function of force. The error threshold length is the contour length where the FWLC- and WLC-predicted extensions differ by 5%. For values of $L < L_e$, the classic WLC solution gives significant errors in the predicted extension. The polymer persistence length is $A = 50$ nm. The error threshold length is largest at low force.

Top: no bead. The different curves correspond to unconstrained, half-constrained, and perpendicular boundary conditions. The more constrained boundary conditions have larger error threshold lengths at low force than the unconstrained boundary condition. Comparable predicted extensions by the classic WLC solution and the FWLC over the range of forces and boundary conditions shown requires $L > 10^4$ nm ($L/A > 200$).

Middle: one bead. The boundary conditions are half-constrained on both ends of the chain. We calculate the extension predicted to the center of the bead, then subtract the bead radius and compare to the extension predicted by the WLC. Larger bead radii lead to larger values of L_e at small forces, while for larger values of the applied force L_e is independent of the bead radius. Comparable predicted extensions by the classic WLC solution and the FWLC over the range of forces and boundary conditions shown requires $L > 8 \times 10^4$ nm ($L/A > 1600$).

Bottom: two beads. The boundary conditions are half-constrained on both ends of the chain. We calculate the extension predicted between the centers of the beads, then subtract twice the bead radius and compare to the extension predicted by the WLC. Larger bead radii lead to larger values of L_e at small forces, while for larger values of the applied force, L_e is independent of the bead radius. The values of L_e are larger for the two-bead case than the one-bead case. Comparable predicted extensions by the classic WLC solution and the FWLC over the range of forces and boundary conditions shown requires $L > 10^5$ nm ($L/A > 2000$).

Figure 8.

Force-extension curves predicted by the FWLC model for $L = 200$ nm ($L/A = 4$).

Top: no bead. The different curves correspond to the classic WLC solution and the FWLC with unconstrained, half-constrained, and perpendicular boundary conditions. The predicted extension for all boundary conditions converges at high force. For low applied force, the more constrained boundary conditions lead to larger predicted extension (see text).

Middle: one bead. The different curves correspond to bead radii of 100, 250, and 500 nm. The predicted molecule extension (after the bead radius has been subtracted) agrees with the no-bead prediction for large force, but decreases more rapidly as the force decreases. For low applied force (below 0.05 pN) the predicted extension becomes negative, because the bead-wall exclusion interaction is neglected in the model. In this regime the theory gives unphysical predictions.

Bottom: two beads. The different curves correspond to bead radii of 100, 250, and 500 nm. The predicted molecule extension (after twice the bead radius has been subtracted) agrees with the no-bead and one-bead predictions for large force. For low applied force (below 0.08 pN) the predicted extension becomes negative, because the bead-bead exclusion interaction is neglected in the model. In this regime the theory gives unphysical predictions.

Figure 9.

Force-extension curves predicted by the FWLC model for $L = 500$ nm ($L/A = 10$). Compared to the curves for $L = 200$ nm (figure 8) the effects of boundary conditions and beads are less important.

Top: no bead. The different curves correspond to the classic WLC solution and the FWLC with unconstrained, half-constrained, and perpendicular boundary conditions.

Middle: one bead. The different curves correspond to bead radii of 100, 250, and 500 nm. For low applied force (below 0.02 pN) the predicted extension becomes negative, because the bead-wall exclusion interaction is neglected in the model. In this regime the theory gives unphysical predictions.

Bottom: two beads. The different curves correspond to bead radii of 100, 250, and 500 nm. For low applied force (below 0.06 pN) the predicted extension becomes negative, because the bead-bead exclusion interaction is neglected in the model. In this regime the theory gives unphysical predictions.

Figure 10.

Results of fitting the FWLC model predictions to the classic WLC solution. The fit value of the persistence length is shown as a function of contour length L . The polymer persistence length is $A = 50$ nm.

Top: no bead. The different curves correspond to the unconstrained, half-constrained, and perpendicular boundary conditions. The apparent A decreases most for the half-constrained boundary conditions. The apparent persistence length decreases by more than a factor of two as L decreases from 10^4 to 100 nm.

Middle: one bead. The different curves correspond to bead radii of 100, 250, and 500 nm. The decrease in the apparent persistence length is similar to that shown in the top panel, half-constrained boundary conditions.

Bottom: two beads. The different curves correspond to bead radii of 100, 250, and 500 nm. The apparent persistence length decreases more quickly with contour length than for the one-bead case.

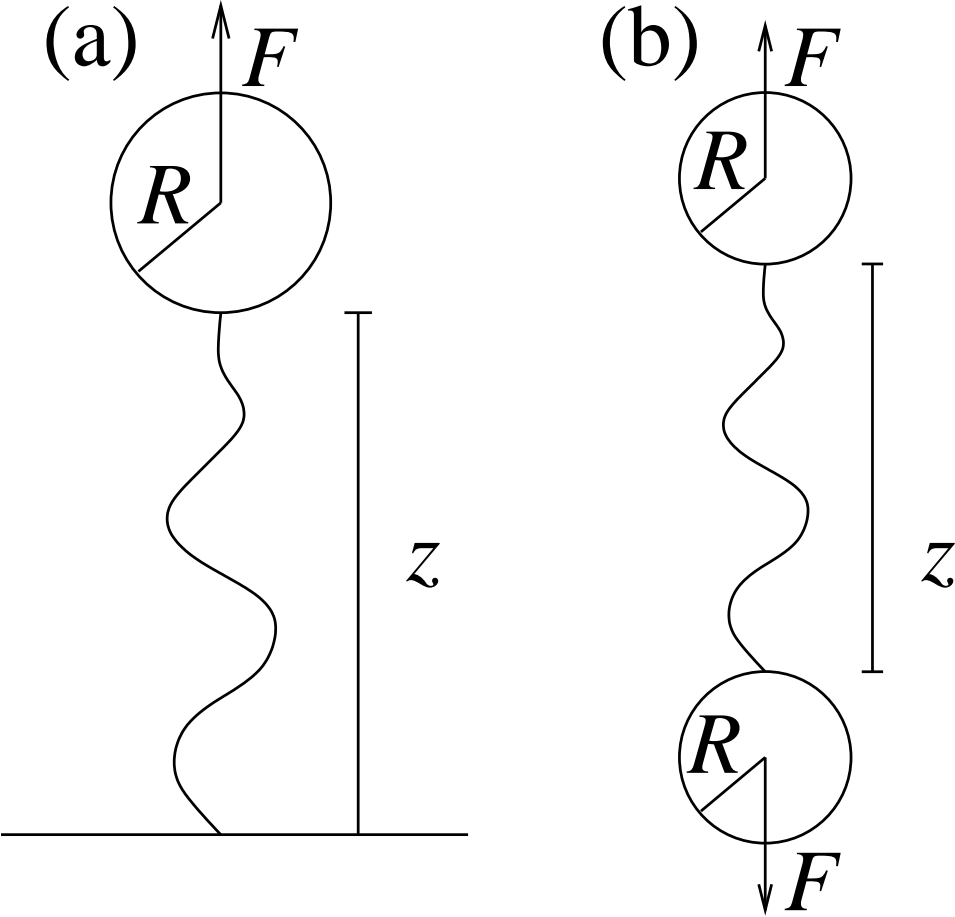


Figure 1:

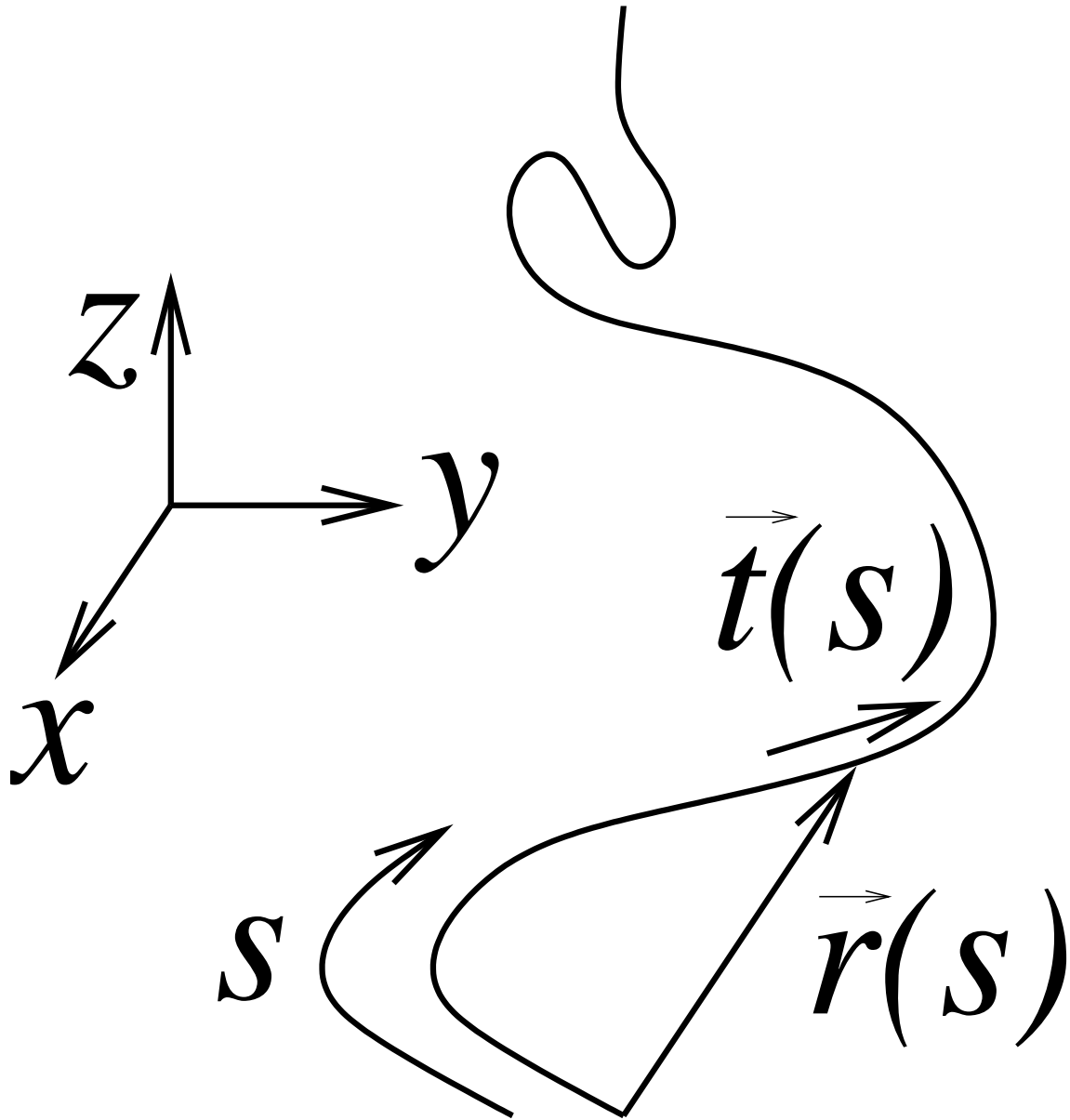


Figure 2:

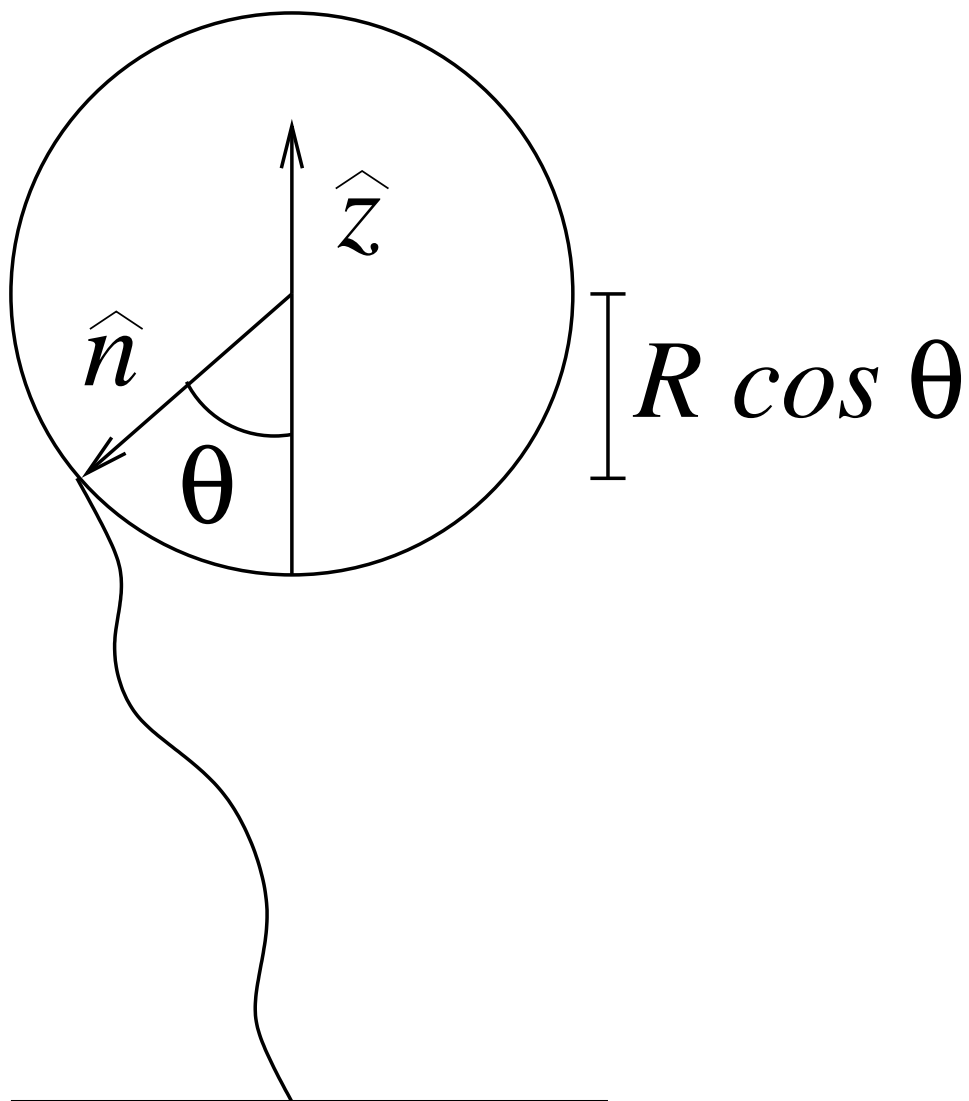


Figure 3:

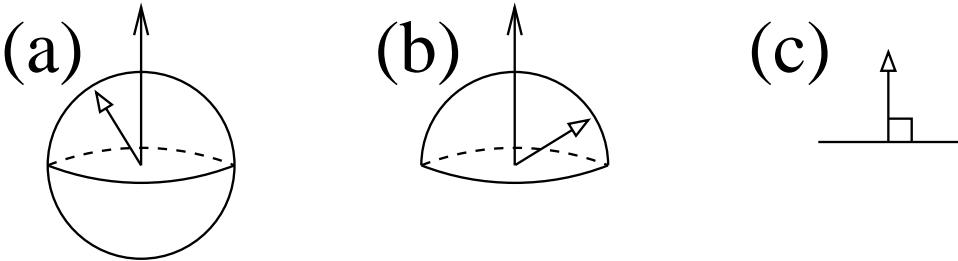


Figure 4:

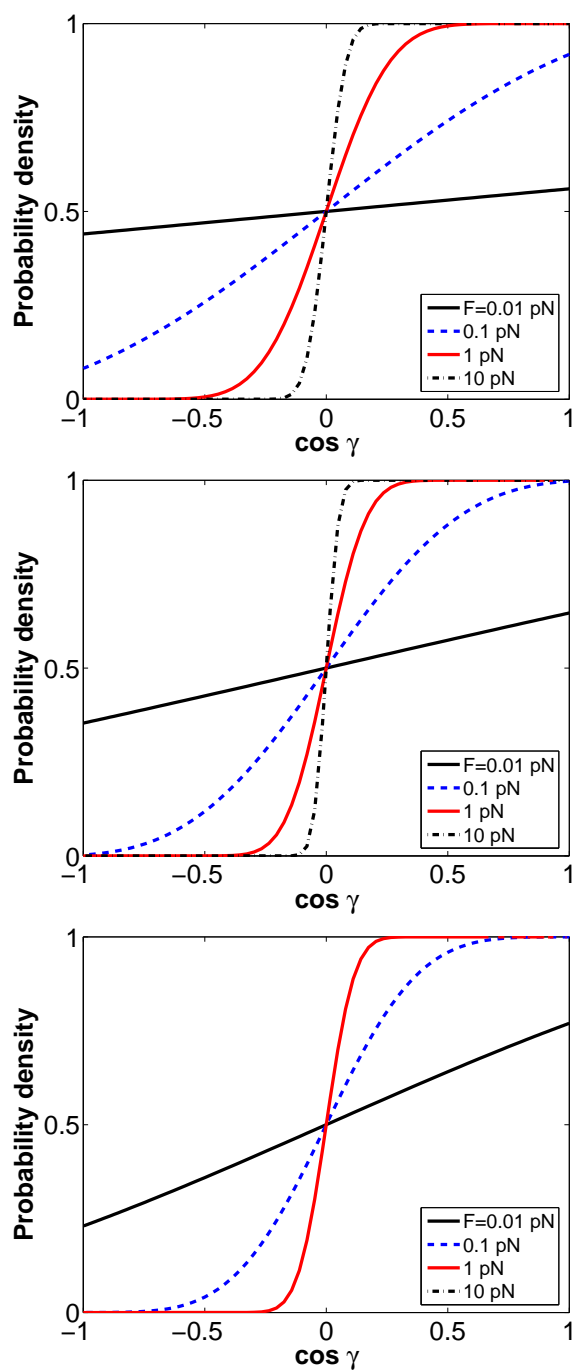


Figure 5:

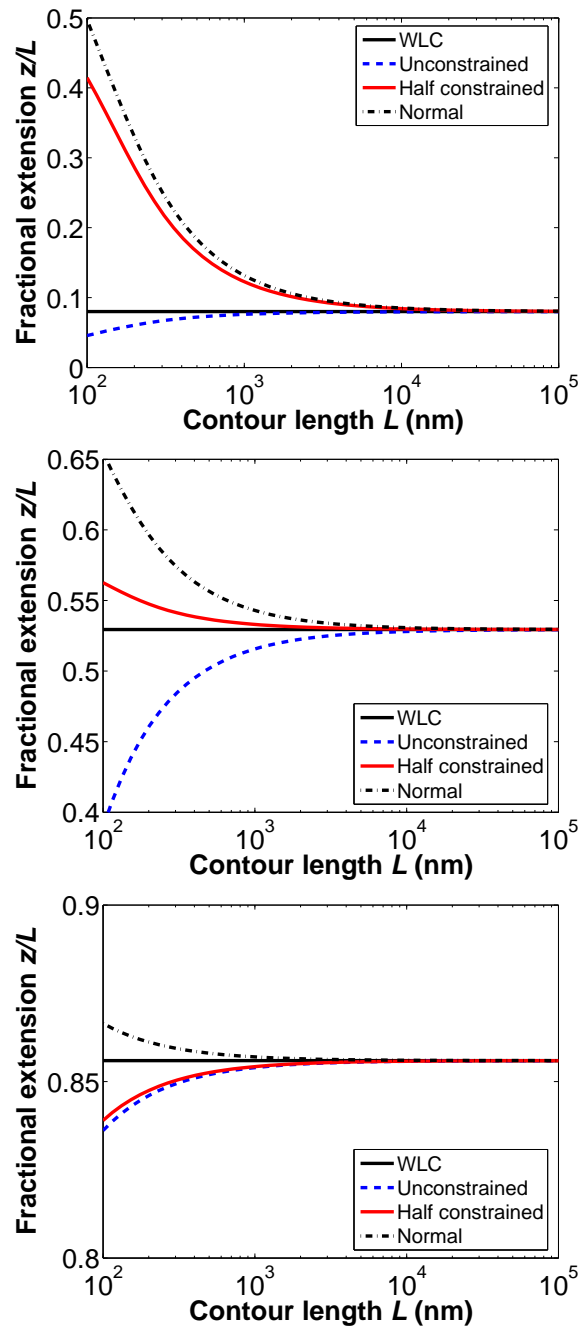


Figure 6:

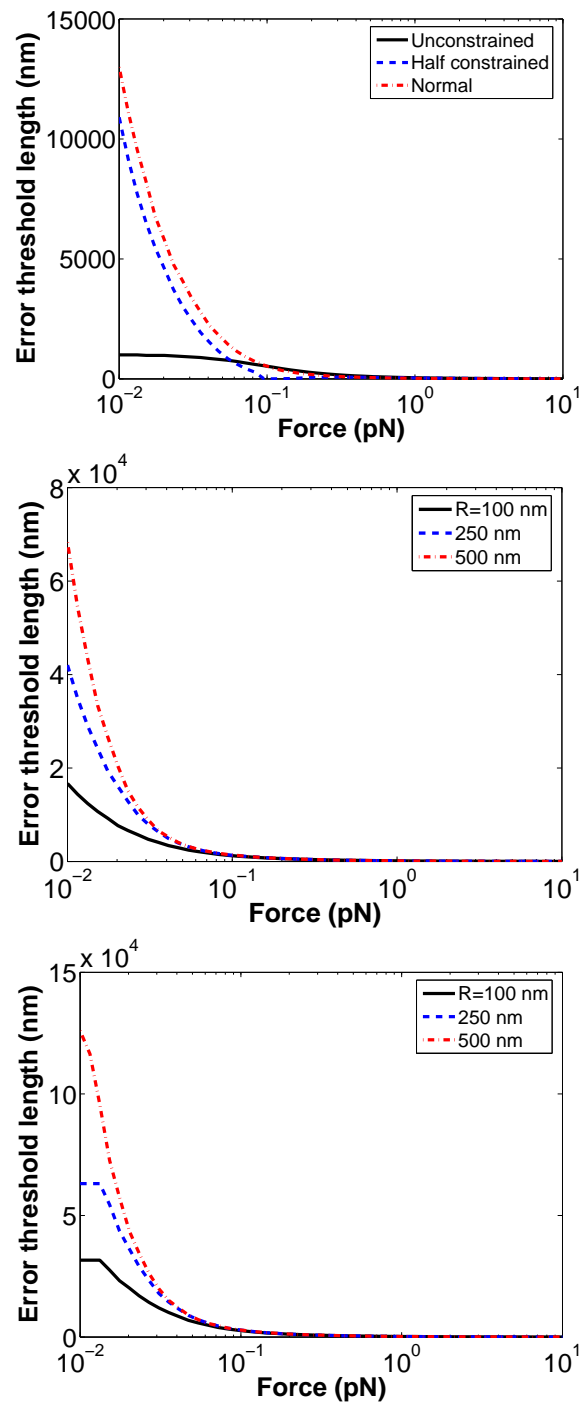


Figure 7:

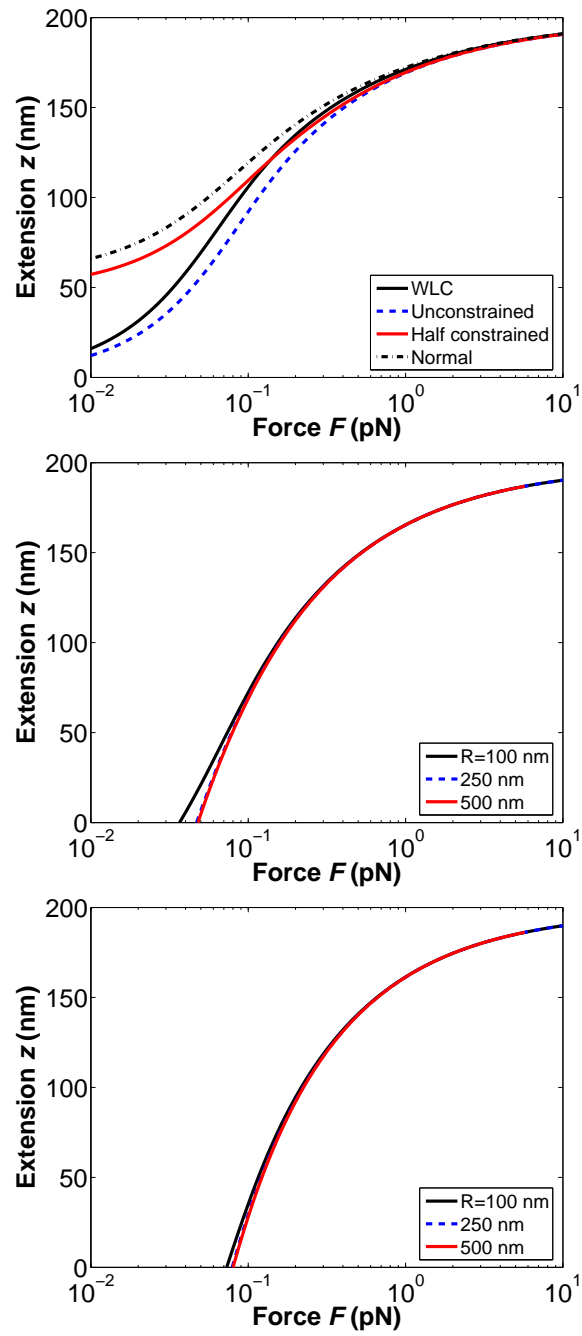


Figure 8:

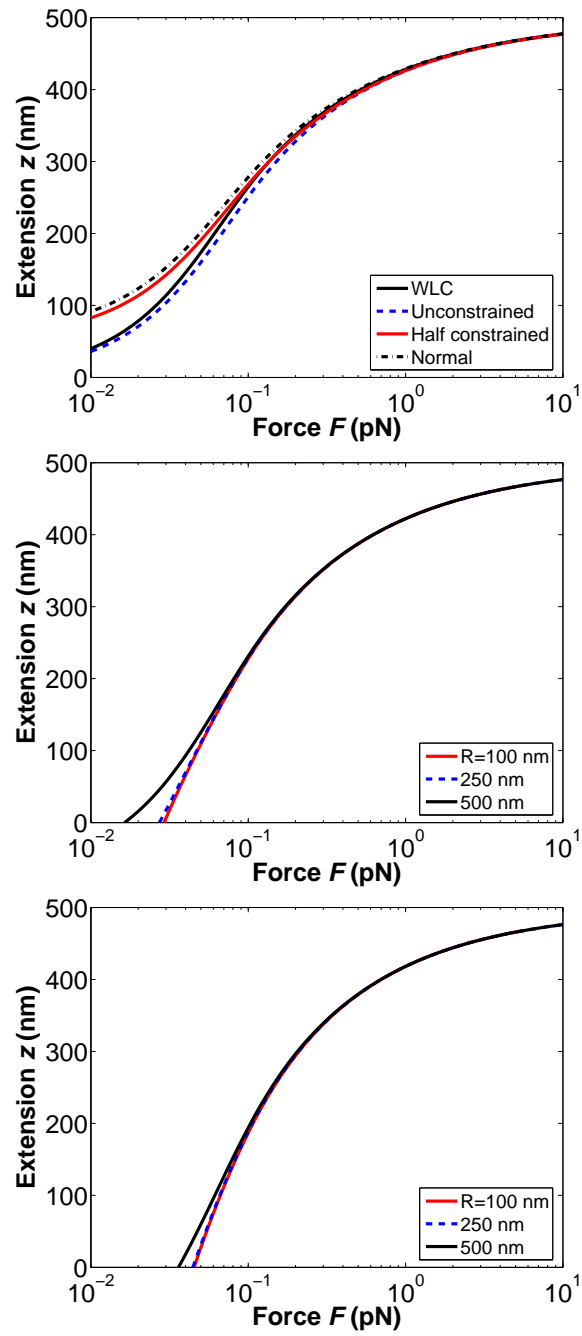


Figure 9:

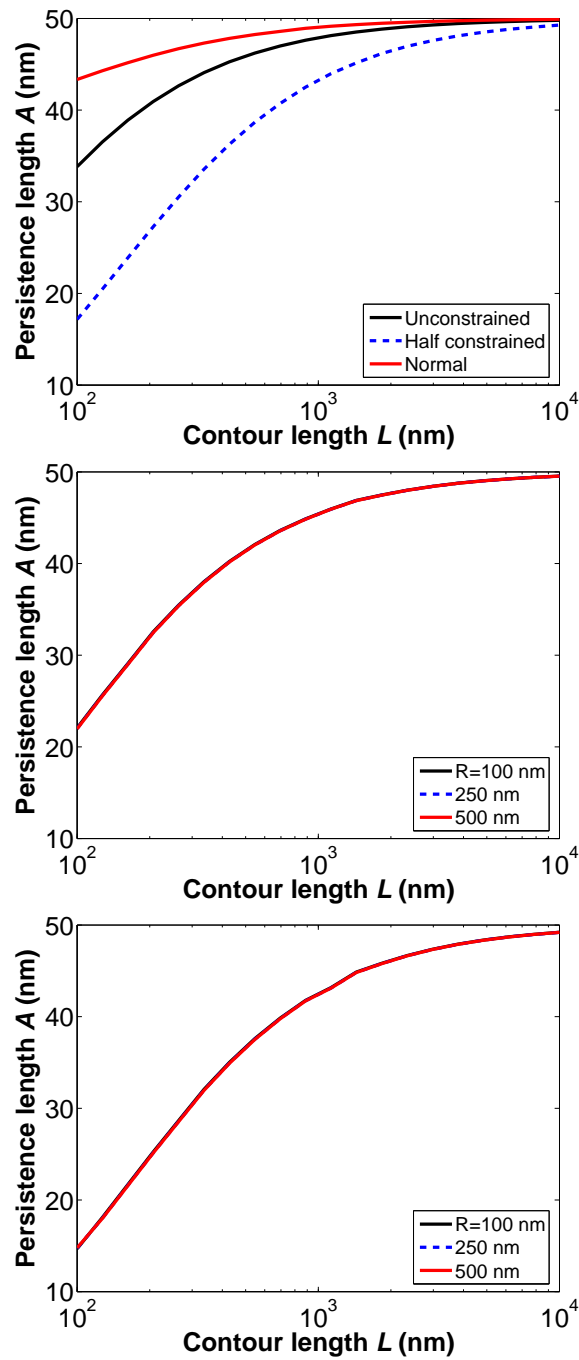


Figure 10: